New Results for Pearson Type III Family of Distributions and Application in Wireless Power Transfer

Sotiris A. Tegos, *Student Member, IEEE*, George K. Karagiannidis, *Fellow, IEEE*, Panagiotis D. Diamantoulakis, *Senior Member, IEEE*, and Nestor D. Chatzidiamantis, *Senior Member, IEEE*

***Abstract*—The Pearson type III and the log Pearson type III distributions have been considered in several scientific fields, as in hydrology and seismology. In this article, we present new results for these distributions and we utilize them, for the first time in the literature, to investigate the statistical behavior of wireless power transfer, which can prolong the lifetime of Internet of Things networks, considering the nonlinear relationship between the received and harvested power, which can be precisely modeled by using the logistic function. Specifically, we present new closed-form expressions for the statistical properties of a general form of the Pearson type III and the log Pearson type III distributions and we utilize them to introduce a new member of the Pearson type III family, the logit Pearson type III distribution, through which the logit gamma and the logit exponential distributions are also defined. Moreover, we derive closed-form expressions for the probability density function, the cumulative distribution function and moments of the distributions of the sum, the log sum, and the logit sum of Pearson type III random variables. Furthermore, taking into account that the Pearson type III family of distributions is closely related to the considered nonlinear energy harvesting model the statistical properties of the distribution of the harvested power are derived, for both single input single output and multiple input single output scenarios with or without channel state information at the transmitter.**

***Index Terms*—Energy harvesting (EH), log Pearson type III distribution, logit Pearson type III distribution, Pearson type III distribution, wireless power transfer (WPT).**

I. Introduction

THE PEARSON type III and the log Pearson type III distributions [1]–[4] attracted the interest of the research community, since they have been utilized in several scientific fields, such as hydrology and seismology. Specifically, they are frequently used in hydrology for flood frequency analysis [5], while in [6] the log Pearson type III distribution was applied to flood and maximum rainfall data and its general use in fitting annual rainfall and streamflow sequences, was investigated. Furthermore, in [7] it was found that the log Pearson type III distribution can effectively describe the behavior of the maximum earthquake magnitudes for all ranges and also be applied to evaluate the design magnitudes. Although the Pearson type III and the log Pearson type III distributions have been investigated in the existing literature, a more general form of these distributions is not fully investigated. Moreover, the distributions of the sum and the log sum of Pearson type III random variables (RVs) have not been examined.

Regarding communication systems, the Pearson type III distribution can be considered as a generalized form of the gamma and, thus, the exponential distribution, which are frequently used in wireless communications when Nakagami-m or Rayleigh fading is assumed, respectively. Also, in [8] the outage performance of hybrid automatic repeat requests with incremental redundancy (HARQ-IR) was investigated, through the cumulative distribution function (CDF) of the product of multiple correlated shifted gamma RVs, which is a special case of the Pearson type III distribution. Furthermore, the shifted exponential distribution, which also is a special case of the Pearson type III distribution, was used in [9] to extract the outage capacity in a multicarrier system, whereas in [10] it was proposed to model the headway distance in multihop vehicle to vehicle communications. Finally, in [11] the shifted gamma distribution was used to model long-range dependent Internet traffic, when the input traffic rate is not Gaussian, and in [12] it was also used to extract upper and lower bounds for the channel capacity in neuro-spike communications.

Internet of Things (IoT) leads to the network integration of a huge amount of wireless devices, thus, raising several research and implementation challenges. The priorities of the European Union in the Next Generation IoT (NGIoT) include the development of reliable, low cost, sustainable and scalable wireless networks, IoT miniaturization, energy harvesting (EH), and pervasiveness [13]. EH is a promising solution for prolonging the lifetime of IoT networks by offering self-sustainability to the devices, minimizing, if not eliminating, the use of battery power. This is of paramount importance especially when replacing or recharging the batteries is inconvenient, costly, or dangerous, such as in remote areas and harsh

Manuscript received 7 May 2022; accepted 1 July 2022. Date of publication 7 July 2022; date of current version 21 November 2022. This work was supported by the European Regional Development Fund by the European Union and Greek national funds through the Operational Program Competitiveness, Entrepreneurship, and Innovation under the call: "Special Actions: Aquaculture—Industrial Materials—Open Innovation in Culture" under Project T6YBP-00134. The work of Sotiris A. Tegos was supported by the Hellenic Foundation for Research and Innovation (HFRI) under the HFRI Ph.D. Fellowship Grant (Fellowship Number: 1394). This article was presented in part at the 22th IEEE International Workshop on Signal Processing Advances in Wireless Communications (IEEE SPAWC '21), Lucca, Italy, 2021 [DOI: 10.1109/SPAWC51858.2021.9593175]. *(Corresponding author: Sotiris A. Tegos.)*

The authors are with the Wireless Communication and Information Processing Group, Department of Electrical and Computer Engineering, Aristotle University of Thessaloniki, 54 124 Thessaloniki, Greece (e-mail: tegosoti@auth.gr; geokarag@auth.gr; padiaman@auth.gr; nestoras@auth.gr).

Digital Object Identifier 10.1109/JIOT.2022.3189220

industrial environments, e.g., rotating and moving platforms, human bodies, or vacuum equipment [14]. However, the main disadvantage of basic EH methods is their reliability, since they depend solely on ambient natural energy sources, such as wind and solar, which are uncontrollable. To this end, wireless power transfer (WPT) which utilizes radio frequency (RF) signals for EH is an interesting alternative and also benefits from high-density networks [15], [16]. In future wireless networks where WPT is applied, low-power devices without communication capabilities can be wirelessly powered anytime and anywhere and low-power communication devices, e.g., sensors, can experience a ubiquitous wireless connectivity. To this end, WPT can assist in various communication scenarios, e.g., orthogonal multiple access schemes [17], nonorthogonal multiple access schemes [18], [19], etc.

Scanning the open literature, a linear EH model is frequently used to express the harvested power, when WPT is performed [17], [18], [20]. Although, this model can be easily handled because of its simplicity, it can be considered impractical, since it is not accurate and cannot describe the saturation of the EH circuit, which can occur even when the received power is relatively low [21]. Although, in practical EH circuits, a linear region exists, the operation in this region cannot be assured, since it depends on the transmitted power and the fading. To this end, nonlinear EH models were proposed in [22] and [23]. Also, in [21] a practical parametric nonlinear EH model was proposed and its accuracy was verified through measurements. This model is based on the logistic function and due to its accuracy has been adopted in several research works [24]–[26]. It captures the dynamics of the RF energy conversion efficiency for different input power levels, in contrast with the linear model which is accurate only when the received power is constant. However, although this nonlinear EH model has received the researchers' attention, its statistical properties, e.g., the CDF, the probability density function (PDF), and the moments, have not been derived, which is a prerequisite to analytically evaluate the capabilities and reliability of this technology. Considering that the basis of this model is the logistic function, the analytical investigation of WPT performance, assuming Nakagami-m or Rayleigh fading, is facilitated by the use of the logit Pearson type III distribution, which however has not been defined and studied in the existing literature, in which solely the logit normal distribution has been investigated [27], [28].

A. Contribution

In the present work, we introduce the logit Pearson type III distribution and we utilize the statistical properties of this distribution to investigate the performance of WPT systems where the nonlinear EH model proposed in [21] is considered. The specific contributions of this article are listed as follows.

1) We introduce a new member of the Pearson type III family, the logit Pearson type III distribution, and derive closed-form expressions for its statistical properties, e.g., the CDF, the PDF, and the moments. To this end, first, we provide new results for a general form of the Pearson type III and the log Pearson type III distributions.
2) We derive exact closed-form expressions for the statistical properties of the distribution of the sum, the log sum, and the logit sum of Pearson type III RVs.
3) We utilize the results for the Pearson type III family of distributions to provide a comprehensive analytical framework for the evaluation of the performance of the EH systems, and to analytically evaluate the capabilities and reliability of the WPT technology, taking into account the nonlinear relationship between the received and the harvested power. Useful insights for the EH system can be extracted through the evaluation of the average harvested power and harvested power probability of outage. Both single input single output (SISO) and multiple input single output (MISO) scenarios are considered. Specifically, for the MISO scenario two cases are investigated, i.e., a network with a power beacon (PB) with multiple antennas and a network with multiple PBs with a single antenna. The derived expressions are valid when either perfect channel state information (CSI) or no CSI is available at the PB, which can be considered a practical scenario in machine-type communications (MTCs), where low-power IoT sources perform WPT.

B. Structure

The remainder of the article is organized as follows.

In Section II, the statistical properties of the Pearson type III and the log Pearson type III distribution are derived and the distributions of the sum of Pearson type III and the log sum of Pearson type III RVs are investigated. In Section III, the logit Pearson type III distribution is introduced and its statistical properties are derived as well as the ones of the logit gamma and the logit exponential distributions, and the distribution of the logit sum of Pearson type III RVs. In Section IV, the expressions for the CDF, the PDF, and the moments of the harvested power are derived considering the nonlinear EH model for the SISO and the MISO scenario and simulations are provided. Finally, closing remarks and discussions are provided in Section V.

II. New Results for the Pearson Type III and the Log Pearson Type III Distributions

In this section, the Pearson type III and the log Pearson type III distributions are presented and new results regarding their statistical properties are provided. Also, the distribution of the sum of Pearson type III and log Pearson type III RVs are investigated.

A. Pearson Type III Distribution

If an RV X follows the Pearson type III distribution with parameters (a, b, m), where $a \in \mathbb{R}$ with $a > 0$ is the shape parameter, $b \in \mathbb{R}$ with $b \neq 0$ is the inverse scale parameter and $m \in \mathbb{R}$ is the shift parameter, its PDF is given by [5]

$$f_X(x, a, b, m) = \frac{|b|}{\Gamma(a)}(b(x-m))^{a-1}e^{-b(x-m)} \tag{1}$$

where $\Gamma(\cdot)$ is the gamma function and e is the base of the natural logarithm. If $b > 0$, $x \in (m, +\infty)$ and, if $b < 0$, $x \in (-\infty, m)$.

In the following proposition, the CDF of the Pearson type III distribution is derived for $b < 0$. For $b > 0$, the CDF is provided in [3], but it is also included in the proposition for completeness.

Proposition 1: The CDF of the Pearson type III distribution can be expressed as follows:

$$F_X(x, a, b, m) = \begin{cases} \frac{1}{\Gamma(a)}\Gamma(a, b(x-m)), \ b < 0 \\ \frac{1}{\Gamma(a)}\gamma(a, b(x-m)), \ b > 0 \ [3] \end{cases} \tag{2}$$

where $\Gamma(\cdot, \cdot)$ and $\gamma(\cdot, \cdot)$ are the upper and lower incomplete gamma function, respectively.

Proof: If $b < 0$, $x \in (-\infty, m)$ the CDF is given by

$$F_X(x, a, b, m) = -\frac{b}{\Gamma(a)} \int_{-\infty}^{x} (b(y-m))^{a-1} e^{-b(y-m)} dy. \tag{3}$$

Using $z = b(y - m)$, (3) can be written as follows:

$$F_X(x, a, b, m) = \frac{b}{\Gamma(a)} \int_{b(x-m)}^{\infty} z^{a-1} e^{-z} dy. \tag{4}$$

Considering the definition of the upper incomplete gamma function, the expression of the CDF, when $b < 0$, is derived and the proof is completed. ■

Next, the moments of the Pearson type III distribution are presented. When $b > 0$, the expression for the moments is provided in [3]. We extract the same expression when $b < 0$.

Proposition 2: The nth moment of the Pearson type III distribution is given as follows:

$$\mu_X^n(a, b, m) = \sum_{k=0}^{n} \binom{n}{k} \frac{m^{n-k}\Gamma(k+a)}{b^k \Gamma(a)} \tag{5}$$

where $\binom{n}{k}$ denotes the binomial coefficient.

Proof: If $b < 0$, the nth moment is calculated as follows:

$$\mu_X^n(a, b, m) = \int_{-\infty}^{m} x^n f_X(x, a, b, m) dx. \tag{6}$$

Utilizing the binomial theorem, (6) can be rewritten as

$$\mu_X^n(a, b, m) = \frac{1}{\Gamma(a)} \sum_{k=0}^{n} \binom{n}{k} \frac{m^{n-k}}{b^k} \int_0^{\infty} z^{k+a-1} e^{-z} dz. \tag{7}$$

From the definition of the gamma function, (5) is derived. ■

Corollary 1: From (5), the mean value is obtained as the first moment and can be expressed as follows:

$$\mu_x^1 = \frac{a}{b} + m. \tag{8}$$

The characteristic function of the Pearson type III distribution is given by [5]

$$\phi_X(t) = \frac{e^{jmt}}{\left(1 - \frac{jt}{b}\right)^a} \tag{9}$$

where $j^2 = -1$.

Remark 1: The gamma distribution is a special case of the Pearson type III distribution with $b > 0$ and $m = 0$. If $b \neq 0$, an RV that follows the Pearson type III distribution with parameters (a, b, m) can also be multiplied with a constant c resulting in an RV that follows the Pearson type III distribution with parameters $(a, (b/c), mc)$. Accordingly, if an RV follows the gamma distribution with parameters (a, b) with $b > 0$, multiplying this RV with a negative constant c results in an RV that follows the Pearson type III distribution with parameters $(a, (b/c), 0)$, where the second parameter is negative.

B. Log Pearson Type III Distribution

If the RV X follows the Pearson type III distribution with parameters (a, b, m), the RV $Y = e^X$ follows the log Pearson type III distribution with the same parameters. If $b > 0$, $y \in (e^m, +\infty)$ and, if $b < 0$, $y \in (0, e^m)$. When $b < 0$, the distribution can also be considered as the inverse log Pearson type III.

The PDF of the log Pearson type III distribution is given by [5]

$$f_Y(y, a, b, m) = \frac{|b| e^{bm}}{\Gamma(a)} (b(\ln y - m))^{a-1} y^{-b-1} \tag{10}$$

where $\ln(\cdot)$ is the natural logarithm.

In the following proposition, the CDF of the log Pearson type III distribution is derived for $b < 0$. For $b > 0$, the CDF is provided in [4], but it is also included in the proposition for completeness.

Proposition 3: The CDF of the log Pearson type III distribution can be expressed as follows:

$$F_Y(y, a, b, m) = \begin{cases} \frac{1}{\Gamma(a)}\Gamma(a, b(\ln y - m)), \ b < 0 \\ \frac{1}{\Gamma(a)}\gamma(a, b(\ln y - m)), \ b > 0 \ [4]. \end{cases} \tag{11}$$

Proof: The CDF of the log Pearson type III distribution is derived by integrating (10) or directly from (2). ■

The nth moment of the log Pearson type III distribution is given by [5]

$$\mu_Y^n(a, b, m) = e^{mn} \left(\frac{b}{b-n}\right)^a. \tag{12}$$

If $b > 0$, $b > n$ should be satisfied, whereas, if $b < 0$, there is no constraint.

Corollary 2: From (12), the mean value is obtained as the first moment and can be expressed as follows:

$$\mu_Y^1 = \frac{a}{b} + m. \tag{13}$$

An approximation of the characteristic function of the log Pearson type III distribution, as a formal power series [29], is provided in the following proposition.

Proposition 4: The characteristic function of the log Pearson type III distribution is approximately given as follows:

$$\phi_Y(t) = \sum_{n=0}^{\infty} \frac{\mu_n}{n!} (jt)^n = \sum_{n=0}^{\infty} \frac{e^{mn}}{n!} \left(\frac{b}{b-n}\right)^a (jt)^n \tag{14}$$

where $n!$ is the factorial of n. Equation (14) stands only when $b < 0$.

Corollary 3: The infinite series in (14) converges.

Proof: By setting $c_n = [e^{mn}/n!](b/b-n)^a(jt)^n$, it holds that

$$\lim_{n\to\infty}\left|\frac{c_{n+1}}{c_n}\right| = \lim_{n\to\infty}\left|\frac{e^m jt}{n+1}\left(\frac{b-n}{b-n-1}\right)^a\right| = 0. \quad (15)$$

■

C. Distribution of the Sum of Pearson Type III RVs

In this section, the distribution of the sum of Pearson type III RVs is investigated. Let $\{X_q\}_{q=1}^L$ be a set of L RVs following the Pearson type III distribution with $a_i \in \mathbb{Z}$, $a_i > 0$ and either $b_i > 0 \ \ \forall i$ or $b_i < 0 \ \ \forall i$. The RV $\hat{X}_L$ is defined as the sum of the above set, i.e.,

$$\hat{X}_L = \sum_{i=1}^{L} X_i. \quad (16)$$

If $b_i > 0 \ \ \forall i$, $x \in (\hat{m}_L, \infty)$ and if $b_i < 0 \ \ \forall i$, $x \in (-\infty, \hat{m}_L)$ with $\hat{m}_L = \sum_{i=1}^{L} m_i$.

Proposition 5: The PDF of $\hat{X}_L$ is given by

$$f_{\hat{X}_L}(x) = \begin{cases} f_X(x, \hat{a}_L, b, \hat{m}_L), & b_i = b \quad \forall i \\ \sum_{i=1}^{L}\sum_{k=1}^{a_i} \Xi_L\Big(i, k, \{a_q\}_{q=1}^L, & \{b_q\}_{q=1}^L, \{j_q\}_{q=1}^{L-2}\Big) \\ \times f_{X_i}(x, k, b_i, \hat{m}_L), & b_i \neq b_j \quad \forall i \neq j \end{cases} \quad (17)$$

where the weights Ξ_L are given by (18), shown at the bottom of the page, with $\hat{a}_L = \sum_{i=1}^{L} a_i$ and $U(\cdot)$ being the Heaviside step function defined as $U(x \geq 0) = 1$.

Proof: The proof is provided in Appendix A. ■

Since (18) is complicated, a recursive formula for the calculation of Ξ_L is presented starting from the case that $k = a_i$ [30], [31], i.e.,

$$\Xi_L\Big(i, a_i, \{a_q\}_{q=1}^L, \{b_q\}_{q=1}^L, \{j_q\}_{q=1}^{L-2}\Big) = \frac{\prod_{w=1}^{L} b_w^{a_w}}{b_i^{a_i}} \prod_{\substack{j=1\\ j\neq i}}^{L} (b_j - b_i)^{-a_j}. \quad (19)$$

When the second argument of Ξ_L is $a_i - k$, the value of Ξ_L can be calculated as follows:

$$\Xi_L\Big(i, a_i - k, \{a_q\}_{q=1}^L, \{b_q\}_{q=1}^L, \{j_q\}_{q=1}^{L-2}\Big) = \frac{1}{k}\sum_{j=1}^{k}\sum_{\substack{q=1\\ q\neq i}}^{L} a_q b_i^j (b_i - b_q)^{-j} \times \Xi_L\Big(i, a_i - k + j, \{a_q\}_{q=1}^L, \{b_q\}_{q=1}^L, \{j_q\}_{q=1}^{L-2}\Big). \quad (20)$$

Remark 2: The PDF of $\hat{X}_L$ for the case that at least one $m_i \neq 0$ and $b_i \neq b_j \ \ \forall i \neq j$ can be written as follows:

$$f_{\hat{X}_L}(x) = \sum_{i=1}^{L}\sum_{k=1}^{a_i}\sum_{l=1}^{k} f_{X_i}(x, l, b_i, m_i) \times \tilde{\Xi}_L\Big(i, k, l, \{a_q\}_{q=1}^L, \{b_q\}_{q=1}^L, \{m_q\}_{q=1}^L, \{j_q\}_{q=1}^{L-2}\Big) \quad (21)$$

where the weights $\tilde{\Xi}_L$ are given by (22), shown at the bottom of the page. It should be highlighted that the PDF of $\hat{X}_L$ in (21) is a nested finite weighted sum of Pearson type III PDFs.

Proof: Utilizing the binomial theorem in (17), (21) can be derived. ■

In the following proposition, the CDF of the distribution of the sum of Pearson type III RVs is provided.

Proposition 6: The CDF of $\hat{X}_L$ is given by

$$F_{\hat{X}_L}(x) = \begin{cases} F_X(x, \hat{a}_L, b, \hat{m}_L), & b_i = b \quad \forall i \\ \sum_{i=1}^{L}\sum_{k=1}^{a_i} \Xi_L\Big(i, k, \{a_q\}_{q=1}^L, & \{b_q\}_{q=1}^L, \{j_q\}_{q=1}^{L-2}\Big) \\ \times F_{X_i}(x, k, b_i, \hat{m}_L), & b_i \neq b_j \quad \forall i \neq j. \end{cases} \quad (23)$$

$$\begin{aligned}\Xi_L\Big(i, k, \{a_q\}_{q=1}^L, \{b_q\}_{q=1}^L, \{j_q\}_{q=1}^{L-2}\Big) &= \sum_{j_1=k}^{a_i}\sum_{j_2=k}^{n_1}\cdots\sum_{j_{L-2}=k}^{j_{L-3}} (-1)^{\hat{a}_L - a_i}\frac{\prod_{w=1}^{L} b_w^{a_w}}{b_i^k}\frac{(a_i + a_{1+U(1-i)} - j_1 - 1)!}{(a_{1+U(1-i)} - 1)!(a_i - j_1)!} \\ &\times (b_i - b_{1+U(1-i)})^{j_1 - a_i - a_{1+U(1-i)}}\frac{(j_{L-2} + a_{L-1+U(L-1-i)} - k - 1)!}{(a_{L-1+U(L-1-i)} - 1)!(j_{L-2} - k)!}(b_i - b_{L-1+U(L-1-i)})^{k - j_{L-2} - a_{L-1+U(L-1-i)}} \\ &\times \prod_{s=1}^{L-3}\frac{(j_s + a_{s+1+U(s+1-i)} - j_{s+1} - 1)!(b_i - b_{s+1+U(s+1-i)})^{j_{s+1} - j_s - a_{s+1+U(s+1-i)}}}{(a_{s+1+U(s+1-i)} - 1)!(j_s - j_{s+1})!}\end{aligned} \quad (18)$$

$$\begin{aligned}\tilde{\Xi}_L\Big(i, k, l, \{a_q\}_{q=1}^L, \{b_q\}_{q=1}^L, \{m_q\}_{q=1}^L, \{j_q\}_{q=1}^{L-2}\Big) &= \sum_{j_1=k}^{a_i}\sum_{j_2=k}^{n_1}\cdots\sum_{j_{L-2}=k}^{j_{L-3}} \frac{e^{(\hat{m}_L - m_i)b_i}(m_i - \hat{m}_L)^{k-l}}{(k-l)!}(-1)^{\hat{a}_L - a_i}\frac{\prod_{w=1}^{L} b_w^{a_w}}{b_i^l} \\ &\times \frac{(a_i + a_{1+U(1-i)} - j_1 - 1)!}{(a_{1+U(1-i)} - 1)!(a_i - j_1)!}(b_i - b_{1+U(1-i)})^{j_1 - a_i - a_{1+U(1-i)}}\frac{(j_{L-2} + a_{L-1+U(L-1-i)} - k - 1)!}{(a_{L-1+U(L-1-i)} - 1)!(j_{L-2} - k)!} \\ &\times (b_i - b_{L-1+U(L-1-i)})^{k - j_{L-2} - a_{L-1+U(L-1-i)}}\prod_{s=1}^{L-3}\frac{(j_s + a_{s+1+U(s+1-i)} - j_{s+1} - 1)!(b_i - b_{s+1+U(s+1-i)})^{j_{s+1} - j_s - a_{s+1+U(s+1-i)}}}{(a_{s+1+U(s+1-i)} - 1)!(j_s - j_{s+1})!}\end{aligned} \quad (22)$$

Proof: The CDF of $\hat{X}_L$ can be obtained by integrating (17) from $\hat{m}_L$ to x, interchanging the order of summation and integration and utilizing (2). ■

Next, closed-form expression for the moments the distribution of the sum of Pearson type III RVs are provided.

Proposition 7: The nth moment of $\hat{X}_L$ is given by

$$\mu^n_{\hat{X}_L} = \begin{cases} \mu^n_X(\hat{a}_L, b, \hat{m}_L), & b_i = b \quad \forall i \\ \sum_{i=1}^{L}\sum_{k=1}^{a_i} \Xi_L\Big(i, k, \{a_q\}_{q=1}^{L}, & \{b_q\}_{q=1}^{L}, \{j_q\}_{q=1}^{L-2}\Big) \\ \times \mu^n_X(k, b, \hat{m}_L), & b_i \neq b_j \quad \forall i \neq j. \end{cases} \tag{24}$$

Proof: The nth moment of $\hat{X}_L$ can be obtained by the integrals $\int_{-\infty}^{\hat{m}_L} x^n f_{\hat{X}_L}(x)dx$ if $b_i < 0$ $\forall i$ and $\int_{\hat{m}_L}^{\infty} x^n f_{\hat{X}_L}(x)dx$ if $b_i > 0$ $\forall i$, by interchanging the order of summation and integration and utilizing (5). ■

D. Distribution of the Log Sum of Pearson Type III RVs

In this section, the distribution of the log sum of Pearson type III RVs is investigated. If the RV $\hat{X}_L$ is a sum of Pearson type III RVs, the RV $\hat{Y}_L = e^{\hat{X}_L}$ follows the distribution of the log sum of Pearson type III RVs. If $b_i > 0$ $\forall i$, $y \in (e^{\hat{m}_L}, +\infty)$ and, if $b_i < 0$ $\forall i$, $y \in (0, e^{\hat{m}_L})$.

Proposition 8: The CDF of $\hat{Y}_L$ is given by

$$F_{\hat{Y}_L}(y) = \begin{cases} F_Y(y, \hat{a}_L, b, \hat{m}_L), & b_i = b \quad \forall i \\ \sum_{i=1}^{L}\sum_{k=1}^{a_i} \Xi_L\Big(i, k, \{a_q\}_{q=1}^{L}, & \{b_q\}_{q=1}^{L}, \{j_q\}_{q=1}^{L-2}\Big) \\ \times F_{Y_i}(y, k, b_i, \hat{m}_L), & b_i \neq b_j \quad \forall i \neq j. \end{cases} \tag{25}$$

Proof: The CDF of $\hat{Y}_L$ can be obtained from (23). ■

In the following proposition, the PDF of the distribution of the log sum of Pearson type III RVs is extracted.

Proposition 9: The PDF of $\hat{Y}_L$ is given by

$$f_{\hat{Y}_L}(y) = \begin{cases} f_Y(y, \hat{a}_L, b, \hat{m}_L), & b_i = b \quad \forall i \\ \sum_{i=1}^{L}\sum_{k=1}^{a_i} \Xi_L\Big(i, k, \{a_q\}_{q=1}^{L}, & \{b_q\}_{q=1}^{L}, \{j_q\}_{q=1}^{L-2}\Big) \\ \times f_{Y_i}(y, k, b_i, \hat{m}_L), & b_i \neq b_j \quad \forall i \neq j. \end{cases} \tag{26}$$

Proof: The PDF of $\hat{Y}_L$ can be obtained as the first derivative of (25) and by utilizing (10). ■

Next, the moments of the distribution of the log sum of Pearson type III RVs are provided.

Proposition 10: The nth moment of $\hat{Y}_L$ is given by

$$\mu^n_{\hat{Y}_L} = \begin{cases} \mu^n_Y(\hat{a}_L, b, \hat{m}_L), & b_i = b \quad \forall i \\ \sum_{i=1}^{L}\sum_{k=1}^{a_i} \Xi_L\Big(i, k, \{a_q\}_{q=1}^{L}, & \{b_q\}_{q=1}^{L}, \{j_q\}_{q=1}^{L-2}\Big) \\ \times \mu^n_Y(k, b, \hat{m}_L), & b_i \neq b_j \quad \forall i \neq j. \end{cases} \tag{27}$$

If $b_i > 0$ $\forall i$, $b_i > n$ $\forall i$ should be satisfied, whereas, if $b_i < 0$ $\forall i$, there is no constraint.

Proof: The nth moment of $\hat{Y}_L$ can be obtained by the integrals $\int_{-\infty}^{e^{\hat{m}_L}} y^n f_{\hat{Y}_L}(y)dy$ if $b_i < 0$ $\forall i$ and $\int_{e^{\hat{m}_L}}^{\infty} y^n f_{\hat{Y}_L}(y)dy$ if $b_i > 0$ $\forall i$, by interchanging the order of summation and integration and utilizing (12). ■

III. Logit Pearson Type III Distribution

In this section, we utilize the derived results of the previous section to introduce a new member of the Pearson type III family, the logit Pearson type III distribution, and derive its statistical properties. In [27] and [28], the logit normal distribution is investigated where, considering that the RV A follows the normal distribution, the RV B follows the logit normal distribution, if $A = \text{logit}(B) = \ln(B/1 - B)$ or $B = f(A)$, where $f(x) = (1/1 + e^{-x})$ is the logistic function. Accordingly, in this work, we introduce the logit Pearson type III distribution, which is defined as follows.

Definition 1: The RV $Z = (1/1 + e^{-X})$ follows the logit Pearson type III distribution with parameters (a, b, m), if the RV X follows the Pearson type III distribution with the same parameters or, equivalently, $X = \text{logit}(Z)$. Regarding the domain of z, if $b > 0$, $z \in (1/1 + e^{-m}, 1)$, while, if $b < 0$, $z \in (0, [1/1 + e^{-m}])$.

Proposition 11: The CDF of the logit Pearson type III distribution can be expressed as follows:

$$F_Z(z, a, b, m) = \begin{cases} \frac{1}{\Gamma(a)}\Gamma\Big(a, b\Big(\ln\frac{z}{1-z} - m\Big)\Big), & b < 0 \\ \frac{1}{\Gamma(a)}\gamma\Big(a, b\Big(\ln\frac{z}{1-z} - m\Big)\Big), & b > 0. \end{cases} \tag{28}$$

Proof: The CDF of the logit Pearson type III distribution is derived by substituting $x = \ln(z/1 - z)$ in (2). ■

In the following proposition, the PDF of Z is extracted.

Proposition 12: The PDF of the logit Pearson type III distribution is given as follows:

$$f_Z(z, a, b, m) = \frac{|b|e^{bm}}{\Gamma(a)}\left(b\left(\ln\frac{z}{1-z} - m\right)\right)^{a-1} \times z^{-b-1}(1-z)^{b-1}. \tag{29}$$

Proof: The PDF of the logit Pearson type III distribution is derived as the first derivative of the CDF given by (28). ■

In Figs. 1 and 2, the CDF and the PDF of the introduced logit Pearson type III distribution are illustrated, respectively. In both figures, we set $m = 0$, thus for negative b, $x \in (0, 0.5)$ and for positive b, $x \in (0.5, 1)$. It should be highlighted that neither PDF nor CDF is defined in 0, 0.5, or 1 and for the case that $m = 0$, the PDF is symmetric around 0.5. It can be observed that the simulations validate the theoretical results.

Proposition 13: The nth moment of the logit Pearson type III distribution when $b > 0$ is given by (30), shown at the bottom of the next page.

Proof: The proof is provided in Appendix B. ■

Corollary 4: The mean value of the logit Pearson type III distribution when $b > 0$ and $m \geq 0$ is given in closed form by

$$\mu^1_Z(a, b, m) = b^a\Phi\big(-e^{-m}, a, b\big) \tag{31}$$

where $\Phi(\cdot, \cdot, \cdot)$ is the Lerch function [32].

Corollary 5: The second moment of the logit Pearson type III distribution when $b > 0$ and $m \geq 0$ is given in closed form by

$$\mu^2_Z(a, b, m) = b^a\big(\Phi\big(-e^{-m}, a-1, b\big) - (b-1)\Phi\big(-e^{-m}, a, b\big)\big). \tag{32}$$

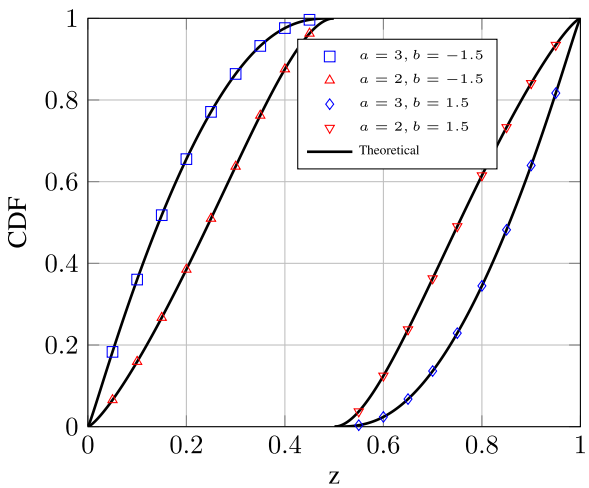

Fig. 1. CDF of the logit Pearson type III distribution.

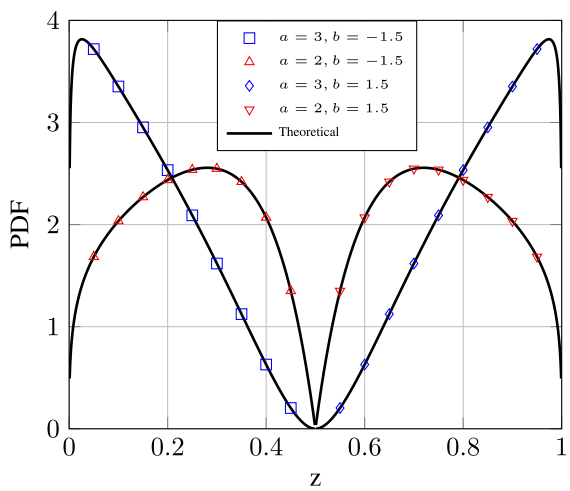

Fig. 2. PDF of the logit Pearson type III distribution.

A. Logit Gamma and the Logit Exponential Distributions

Utilizing the above analysis, for the special case that $b > 0$ and $m = 0$, the logit gamma distribution can be derived. If the RV Z follows the logit gamma distribution, it holds that $z \in (0.5, 1)$, whereas, if we further assume that $a = 1$, the RV Z follows the logit exponential distribution. The CDF of the logit gamma distribution can be expressed as follows:

$$F_Z(z, a, b) = \frac{1}{\Gamma(a)}\gamma\left(a, b\ln\frac{z}{1-z}\right). \tag{33}$$

Similarly, the CDF of the logit exponential distribution is further simplified as follows:

$$F_Z(z, b) = 1 - \left(\frac{z}{1-z}\right)^{-b}. \tag{34}$$

The PDF of the logit gamma distribution is given by

$$f_Z(z, a, b) = \frac{b}{\Gamma(a)}\left(b\ln\frac{z}{1-z}\right)^{a-1} z^{-b-1}(1-z)^{b-1}. \tag{35}$$

Accordingly, the PDF of the logit exponential distribution can be expressed as follows:

$$f_Z(z, b) = bz^{-b-1}(1-z)^{b-1}. \tag{36}$$

The nth moment of the logit gamma distribution is given as follows:

$$\mu_Z^n(a, b) = \sum_{l=0}^{\infty}\binom{n+l-1}{l}(-1)^l\left(1+\frac{l}{b}\right)^{-a}. \tag{37}$$

Corollaries 4 and 5 can be used to extract closed-form expressions for the first and the second moment of the logit gamma distribution. Similarly, the moments of the logit exponential distribution can be derived.

B. Distribution of the Logit Sum of Pearson Type III RVs

In this section, the distribution of the logit sum of Pearson type III RVs is investigated. If the RV $\hat{X}_L$ is a sum of Pearson type III RVs, the RV $\hat{Z}_L = (1/1 + e^{-\hat{X}_L})$ follows the distribution of the logit sum of Pearson type III RVs. If $b_i > 0 \ \ \forall i$, $z \in ([1/1 + e^{-\hat{m}_L}], 1)$ and if $b_i < 0 \ \ \forall i$, $z \in (0, [1/1 + e^{-\hat{m}_L}])$.

Proposition 14: The CDF of $\hat{Z}_L$ is given by

$$F_{\hat{Z}_L}(z) = \begin{cases} F_Z(z, \hat{a}_L, b, \hat{m}_L), & b_i = b \quad \forall i \\ \sum_{i=1}^{L}\sum_{k=1}^{a_i}\Xi_L\Big(i, k, \{a_q\}_{q=1}^{L}, & \{b_q\}_{q=1}^{L}, \{j_q\}_{q=1}^{L-2}\Big) \\ \times F_{Z_i}(z, k, b_i, \hat{m}_L), & b_i \neq b_j \quad \forall i \neq j. \end{cases} \tag{38}$$

Proof: The CDF of $\hat{Z}_L$ can be obtained from (23) by substituting $x = \ln(z/1-z)$. ■

In the following proposition, the PDF of the distribution of the logit sum of Pearson type III RVs is extracted.

Proposition 15: The PDF of $\hat{Z}_L$ is given as follows:

$$f_{\hat{Z}_L}(z) = \begin{cases} f_Z(z, \hat{a}_L, b, \hat{m}_L), & b_i = b \quad \forall i \\ \sum_{i=1}^{L}\sum_{k=1}^{a_i}\Xi_L\Big(i, k, \{a_q\}_{q=1}^{L}, & \{b_q\}_{q=1}^{L}, \{j_q\}_{q=1}^{L-2}\Big) \\ \times f_{Z_i}(z, k, b_i, \hat{m}_L), & b_i \neq b_j \quad \forall i \neq j. \end{cases} \tag{39}$$

Proof: The PDF of $\hat{Z}_L$ can be obtained as the first derivative of (38) and by utilizing (29). ■

Next, the moments of the distribution of the logit sum of Pearson type III RVs are provided.

$$\mu_Z^n(a, b, m) = \begin{cases} \sum_{l=0}^{\infty}\binom{n+l-1}{l}(-1)^l e^{-ml}\left(1+\frac{l}{b}\right)^{-a}, & m \geq 0 \\ \frac{1}{\Gamma(a)}\sum_{l=0}^{\infty}\binom{n+l-1}{l}(-1)^l\Big(e^{m(n+l)}\left(1-\frac{n+l}{b}\right)^{-a}\gamma\left(a, -mb\left(1-\frac{n+l}{b}\right)\right) & \\ \quad +e^{-ml}\left(1+\frac{l}{b}\right)^{-a}\Gamma\left(a, -mb\left(1+\frac{l}{b}\right)\right)\Big), & m < 0 \end{cases} \tag{30}$$

Proposition 16: The nth moment of $\hat{Z}_L$ when $b_i > 0 \quad \forall i$ is given by

$$\mu^n_{\hat{Z}_L} = \begin{cases} \mu^n_Z(\hat{a}_L, b, \hat{m}_L), & b_i = b \quad \forall i \\ \sum_{i=1}^{L} \sum_{k=1}^{a_i} \Xi_L\Big(i, k, \{a_q\}_{q=1}^{L} & \{b_q\}_{q=1}^{L}, \{j_q\}_{q=1}^{L-2}\Big) \\ \times \mu^n_Z(k, b, \hat{m}_L), & b_i \neq b_j \quad \forall i \neq j. \end{cases} \tag{40}$$

Proof: The nth moment of $\hat{Z}_L$ can be obtained by the integral $\int_{(1/1+e^{-\hat{m}_L})}^{1} z^n f_{\hat{Z}_L}(z)dz$ by interchanging the order of summation and integration and utilizing (30). ■

IV. Application of Pearson Type III Family of Distributions in WPT

A. System Model

In this section, a network is considered which consists of one PB or multiple PBs that utilizes WPT to provide energy to the assigned EH sources, e.g., low-power sensors or devices. It is assumed that the harvested power due to the processing noise is negligible and, thus, it can be ignored. The nonlinear EH model proposed in [21] is considered, which captures the dynamics of the RF energy conversion efficiency for different input power levels and is based on the logistic function. Moreover, it is able to capture the joint effect of the nonlinear phenomena caused by hardware constraints, including circuit sensitivity limitations and current leakage. Two scenarios are considered, i.e., an SISO scenario and an MISO one. Also, for the MISO scenario two cases are considered, i.e., a network with a PB with L antennas and a network with L PBs with a single antenna. When multiple antennas in the PB or multiple PBs are considered, the assigned EH sources can harvest power more reliably than the SISO case, since the number of the values of the harvested power that are lower than the sensitivity threshold due to the randomness of the fading reduce. Therefore, the harvested power increases for the MISO scenario.

The power harvested by one of the sources for the SISO scenario can be expressed as follows [21]:

$$Q^S = \frac{P_s\big(1 + e^{AB}\big)}{e^{AB}\big(1 + e^{-A(lp|h|^2 - B)}\big)} - \frac{P_s}{e^{AB}} \tag{41}$$

where P_s denotes the maximum harvested power when the EH circuit is saturated. Also, A and B are positive constants related to the circuit specification such as the resistance, capacitance, and diode turn-on voltage. Specifically, A reflects the nonlinear charging rate with respect to the input power and B is related to the turn-on threshold. Practically, the parameters P_s, A, and B can be determined by curve fitting, ensuring a zero-input zero-output response for EH. Furthermore, l, p, and h denote the path loss factor between the PB and the source, the transmitted power and the small-scale fading coefficient between the PB and the source, respectively. We assume that the channel fading between the PB and the source is a stationary and ergodic random process, whose instantaneous channel realizations follow the Nakagami-m distribution with parameters $(a, [a/b])$, since the Nakagami-m channel model is general enough to describe the typical wireless fading environments. In this case, $|h|^2$ follows the gamma distribution with parameters (a, b) or the Pearson type III distribution with parameters $(a, b, 0)$.

The power harvested by one of the sources for the MISO scenario can be expressed as follows:

$$Q^M = \frac{P_s\big(1 + e^{AB}\big)}{e^{AB}\Big(1 + e^{-A\left(wp\sum_{i=1}^{L} l_i|h_i|^2 - B\right)}\Big)} - \frac{P_s}{e^{AB}} \tag{42}$$

where

$$w = \begin{cases} 1, & \text{perfect CSI} \\ \frac{1}{L}, & \text{no CSI.} \end{cases} \tag{43}$$

As (43) reveals, (42) expresses the harvested power by a source, when either perfect CSI or no CSI is available at the PB which constitutes a practical case in NGIoT MTC scenarios. Specifically, if perfect CSI is available at the PB and under the sum power constraint, the optimal beamforming is performed, i.e., all antennas transmit the same symbol weighted by a specific complex weight at each antenna. The weight of each antenna has both the phase matched to the phase of the corresponded channel coefficient and the amplitude proportional to the amplitude of this channel coefficient [33], [34]. On the other hand, if CSI is not available at the PB, the transmitted power is equally allocated to the antennas [35], [36]. It should be highlighted that the distribution of the sum of Pearson type III RVs appears and, thus, the distributions presented in Sections II and III can be utilized. In the case that the network consists of one PB with L antennas, it holds that $(b_i/l_i) = (b/l)$ $\forall i$, since the antennas are co-located. In the second case, where the network consists of L PBs with one antenna, considering that the distance between the EH source and each PB is different, it is assumed that $(b_i/l_i) \neq (b_j/l_j) \quad \forall i \neq j$. It should be highlighted that (42) with $w = 1$ is also valid for a single input multiple output scenario where a maximum ratio combiner is utilized in the receiver and the network consists of one EH source with L antennas. However, in practical networks the EH sources are low-cost and low-power devises such as sensors, thus the MISO scenarios are emphasized.

B. Statistical Properties

In this section, we utilize the results extracted in the previous sections to provide the statistical properties of the harvested power.

1) SISO: Some important statistical properties of the distribution of the harvested power for the SISO case are presented as follows.

Theorem 1: The CDF of the distribution of the harvested power for the SISO case is given as follows:

$$F_{Q^S}(q) = \frac{1}{\Gamma(a)}\gamma\Bigg(a, -\frac{b}{Alp} \times \left(\ln\left(\frac{P_s\big(1 + e^{AB}\big)}{e^{AB}\Big(q + \frac{P_s}{e^{AB}}\Big)} - 1\right) - AB\right)\Bigg). \tag{44}$$

Proof: In (41), $|h|^2$ follows the gamma distribution with parameters (a, b), which is also the Pearson type III distribution with parameters $(a, b, 0)$, and $lp|h|^2$ follows the Pearson type III distribution with parameters $(a, (b/lp), 0)$. Therefore, $-A(lp|h|^2-B)$ follows the Pearson type III distribution with parameters $(a, -(b/Alp), AB)$, $e^{-A(lp|h|^2-B)}$ follows the log Pearson type III distribution with the same parameters, and $(1/[1+e^{-A(lp|h|^2-B)}])$ follows the logit Pearson type III distribution with parameters $(a, (b/Alp), -AB)$.

The CDF of the distribution of the harvested power is obtained as follows:

$$F_{Q^S}(q) = \Pr(Q < q) \tag{45}$$

where Pr denotes probability. After some algebraic manipulations and using (28), (45) can be rewritten as follows:

$$F_{Q^S}(q) = F_Z\left(\frac{e^{AB}\left(q+\frac{P_s}{e^{AB}}\right)}{P_s\left(1+e^{AB}\right)}\right). \tag{46}$$

From (46), (44) is derived, which completes the proof. ■

Remark 3: It should be highlighted that the CDF of the distribution of the harvested power indicates the probability that outage occurs in the harvested power if we consider a threshold q.

In the following theorem, the PDF of Q^S is extracted.

Theorem 2: The PDF of the distribution of the harvested power for the SISO case can be expressed as follows:

$$f_{Q^S}(q) = \frac{c\left(1+e^{AB}\right)\hat{b}^a}{\Gamma(a)e^{AB\hat{b}}}\left(ce^{AB}-q\right)^{-1+\hat{b}}(c+q)^{-1-\hat{b}} \times \left(AB - \ln\left(\frac{c\left(1+e^{AB}\right)}{c+q}-1\right)\right)^{a-1} \tag{47}$$

where $\hat{b} = (b/Alp)$ and $c = (P_s/e^{AB})$.

Proof: The PDF is obtained as the first derivative of the CDF given by (44). ■

In the following theorem, the moments of Q^S are provided.

Theorem 3: The nth moment of the distribution of the harvested power for the SISO case is given, if $\hat{b} \notin \mathbb{Z}$, by

$$\begin{aligned}\mu^n_{Q^S} = {} & \frac{c^n}{\Gamma(a)}\sum_{l_1=0}^{n}\sum_{l_2=0}^{\infty}\binom{n}{l_1}\binom{l_1+l_2-1}{l_2}(-1)^{n-l_1+l_2} \\ & \times\left(e^{-AB}+1\right)^{l_1}\left(e^{-ABl_2}\left(1-\frac{l_1+l_2}{\hat{b}}\right)^{-a}\right. \\ & \times\gamma\left(a, AB\hat{b}\left(1-\frac{l_1+l_2}{\hat{b}}\right)\right)+e^{AB(l_1+l_2)} \\ & \left.\times\left(1+\frac{l_2}{\hat{b}}\right)^{-a}\Gamma\left(a, AB\hat{b}\left(1+\frac{l_2}{\hat{b}}\right)\right)\right).\end{aligned} \tag{48}$$

Proof: The proof is provided in Appendix C. ■

Corollary 6: The average harvested power is obtained as the first moment and can be expressed, if $\hat{b} \notin \mathbb{Z}$, as follows:

$$\begin{aligned}\mu^1_{Q^S} = {} & -c + \frac{c\left(1+e^{-AB}\right)}{\Gamma(a)}\sum_{k=0}^{\infty}(-1)^k e^{-ABk} \\ & \left(\left(-\frac{k+1}{\hat{b}}+1\right)^{-a}\gamma\left(a, AB\hat{b}\left(-\frac{k+1}{\hat{b}}+1\right)\right)\right. \\ & \left.+e^{AB(1+2k)}\left(\frac{k}{\hat{b}}+1\right)^{-a}\Gamma\left(a, AB\hat{b}\left(\frac{k}{\hat{b}}+1\right)\right)\right).\end{aligned} \tag{49}$$

In the following remarks, we provide physical insights on the first and second moment of the distribution of the harvested power.

Remark 4: In a WPT system, the average harvested power is of paramount importance, since it can assist in the calculation of the average harvested energy E in a time interval T, i.e., $E = T\mu^1_{Q^S}$. Moreover, in a communication system where WPT is used with an infinite storage capacity battery at the EH source, the average energy departure rate, which represents the average consumed energy, should be less than or equal to the average harvested energy, i.e.,

$$P_t(1-\tau) \le \tau\mu^1_{Q^S} \tag{50}$$

where P_t is the average transmitted power. Moreover, τ is a time-sharing parameter with τT and $(1-\tau)T$ being the duration of the EH phase and the communication phase, respectively, where T is the total time duration. In [37], such a system was considered, but the linear EH model was used, since the average harvested power of the nonlinear model had not been derived.

Remark 5: Utilizing the second moment, the variance of the harvested power can be calculated, which expresses how the values of the harvested power fluctuate around the mean value. It should be highlighted that the variance should be small, so that the majority of the harvested power is larger than the sensitivity threshold of the energy receiver of the EH source.

2) MISO: Accordingly, the statistical properties of the distribution of the harvested power for the MISO case are presented as follows.

Theorem 4: The CDF of the distribution of the harvested power for the MISO case is given as follows:

$$F_{Q^M}(q) = \begin{cases} \frac{1}{\Gamma(\hat{a}_L)}\gamma\left(\hat{a}_L, -\frac{b_i}{Awpl_i}\right. \\ \qquad \left.\times\left(\ln\left(\frac{P_s\left(1+e^{AB}\right)}{e^{AB}\left(q+\frac{P_s}{e^{AB}}\right)}-1\right)-AB\right)\right) \\ \qquad \frac{b_i}{l_i} = \frac{b}{l} \quad \forall i \\ \sum_{i=1}^{L}\sum_{k=1}^{a_i}\frac{1}{\Gamma(k)}\gamma\left(k, -\frac{b_i}{Awpl_i}\right. \\ \qquad \left.\times\left(\ln\left(\frac{P_s\left(1+e^{AB}\right)}{e^{AB}\left(q+\frac{P_s}{e^{AB}}\right)}-1\right)-AB\right)\right) \\ \times\ \Xi_L\left(i, k, \{a_q\}_{q=1}^{L}, \{b_q\}_{q=1}^{L}, \{j_q\}_{q=1}^{L-2}\right) \\ \qquad \frac{b_i}{l_i} \neq \frac{b_j}{l_j} \quad \forall i \neq j. \end{cases} \tag{51}$$

Proof: The CDF of the distribution of the harvested power for the MISO case is obtained considering that $\sum_{i=1}^{L} l_i|h_i|^2$ is a sum of Pearson type III RVs and utilizing (23) and (44). ■

Similarly with the SISO case, the CDF of the distribution of the harvested power for the MISO case indicates outage probability for the harvested power.

In the next theorem, the PDF of Q^M is extracted.

Theorem 5: The PDF of the distribution of the harvested power for the MISO case can be expressed as follows:

$$f_{Q^M}(q) = \begin{cases} \frac{c(1+e^{AB})\hat{b}_i^{\hat{a}_L}}{\Gamma(\hat{a}_L)e^{AB\hat{b}_i}}\left(ce^{AB}-q\right)^{-1+\hat{b}_i}(c+q)^{-1-\hat{b}_i} \\ \quad \times\left(AB-\ln\left(\frac{c(1+e^{AB})}{c+q}-1\right)\right)^{\hat{a}_L-1} \\ \quad \frac{b_i}{l_i}=\frac{b}{l} \quad \forall i \\ \sum_{i=1}^{L}\sum_{k=1}^{a_i}\Xi_L\left(i,k,\{a_q\}_{q=1}^{L},\{b_q\}_{q=1}^{L},\{j_q\}_{q=1}^{L-2}\right) \\ \quad \times\frac{c(1+e^{AB})\hat{b}_i^{k}}{\Gamma(k)e^{AB\hat{b}_i}}\left(ce^{AB}-q\right)^{-1+\hat{b}_i}(c+q)^{-1-\hat{b}_i} \\ \quad \times\left(AB-\ln\left(\frac{c(1+e^{AB})}{c+q}-1\right)\right)^{k-1} \\ \quad \frac{b_i}{l_i}\neq\frac{b_j}{l_j} \quad \forall i\neq j \end{cases} \tag{52}$$

where $\hat{b}_i = (b_i/Awpl_i)$.

Proof: The PDF is obtained as the first derivative of the CDF given by (51). ■

In the following theorem, the moments of Q^M are provided.

Theorem 6: The nth moment of the distribution of the harvested power for the MISO case is given, if $\hat{b}_i \notin \mathbb{Z}$, by (53), shown at the bottom of the page.

Proof: The nth moment is obtained by utilizing (48) and (52). ■

C. Simulation Results

In this section, simulations are provided to validate the theoretical results derived in the previous section. In Figs. 3–7, the performance of the considered EH system is illustrated. The path loss factor is given by $l = (1/d^{\alpha})$, where d and α denote the distance between the transmitter and the receiver and the path loss exponent, respectively, [34]. For the parameters of the nonlinear EH model, we set $A = 150$, $B = 0.014$, and $P_s = 24$ mW [38]. Moreover, we set $a_i = 3\ \forall i$, $b_i = 1\ \forall i$, and the path loss exponent $\alpha = 2.5$ [34], which can be considered as a typical value for MTC scenarios of the NGIoT.

In Fig. 3, the considered nonlinear model proposed in [21] is compared with the linear model where the harvested power is given by $Q_1 = \zeta P_r$ with ζ and P_r denoting the energy conversion efficiency and the received power, respectively, and the nonlinear model proposed in [22] where the harvested power is given by $Q_2 = (aP_r + b/P_r + c) - (b/c)$ with a, b, and c being constants determined by standard curve fitting. The experimental data from a practical EH circuit provided in [39] are also illustrated. For the linear model $\zeta = 0.8$ and for the nonlinear model in [22] we set $a = 4.385$, $b = 0.178$, and $c = 0.041$. It can be observed that although the linear region is well approximated, the saturation of a practical EH circuit, as illustrated by the measurement data, cannot be described by the linear model which highlights its impracticality. Moreover, the nonlinear model proposed in [22] does not fit well in these data, since neither the linear region nor the saturation are well approximated. To this end, the performance of the three EH models cannot be fairly compared.

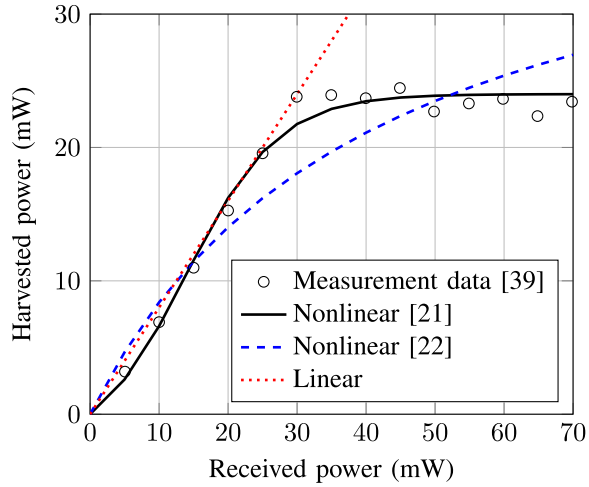

Fig. 3. Comparison of EH models.

In Figs. 4 and 5, the outage probability is illustrated, obtained by (44) and (51) for the SISO and the MISO case, respectively. The outage threshold q_t, which expresses the minimal power needed to be harvested for the operation of the EH source, e.g., circuit consumption, decoding information, or information transmission, is normalized with respect to the maximum harvested power when the power harvesting circuit is saturated, termed as P_s. Figs. 4 and 6 illustrate the performance of the first MISO scenario versus the distance between the PB and the EH source and we set $wp = 2$ W. Figs. 5 and 7 illustrate the performance of the second MISO scenario versus the power wp and the distances between the EH source and the three PBs are 11, 10, and 9 m, respectively.

In Figs. 4 and 5, the outage performance improves significantly, as L increases, since if a link undergoes bad channel conditions, outage may not occur due to the other available links. This cannot be the case when only one antenna is used. Moreover, it can be observed that the slope of the lines is

$$\mu_{Q^M}^{n} = \begin{cases} \frac{c^n}{\Gamma(\hat{a}_L)}\sum_{l_1=0}^{n}\sum_{l_2=0}^{\infty}\binom{n}{l_1}\binom{l_1+l_2-1}{l_2}(-1)^{n-l_1+l_2}\left(e^{-AB}+1\right)^{l_1}\left(e^{-ABl_2}\left(1-\frac{l_1+l_2}{\hat{b}}\right)^{-\hat{a}_L}\right. \\ \quad \left.\times\gamma\left(\hat{a}_L, AB\hat{b}\left(1-\frac{l_1+l_2}{\hat{b}}\right)\right)+e^{AB(l_1+l_2)}\left(1+\frac{l_2}{\hat{b}}\right)^{-\hat{a}_L}\Gamma\left(\hat{a}_L, AB\hat{b}\left(1+\frac{l_2}{\hat{b}}\right)\right)\right), \quad \frac{b_i}{l_i}=\frac{b}{l} \quad \forall i \\ \sum_{i=1}^{L}\sum_{k=1}^{a_i}\sum_{l_1=0}^{n}\sum_{l_2=0}^{\infty}\Xi_L\left(i,k,\{a_q\}_{q=1}^{L},\{b_q\}_{q=1}^{L},\{j_q\}_{q=1}^{L-2}\right)\frac{c^n}{\Gamma(k)}\binom{n}{l_1}\binom{l_1+l_2-1}{l_2}(-1)^{n-l_1+l_2}\left(e^{-AB}+1\right)^{l_1} \\ \quad \times\left(e^{-ABl_2}\left(1-\frac{l_1+l_2}{\hat{b}_i}\right)^{-k}\gamma\left(k, AB\hat{b}_i\left(1-\frac{l_1+l_2}{\hat{b}_i}\right)\right)+e^{AB(l_1+l_2)}\left(1+\frac{l_2}{\hat{b}_i}\right)^{-k}\Gamma\left(k, AB\hat{b}_i\left(1+\frac{l_2}{\hat{b}_i}\right)\right)\right) \\ \quad \frac{b_i}{l_i}\neq\frac{b_j}{l_j} \quad \forall i\neq j \end{cases} \tag{53}$$

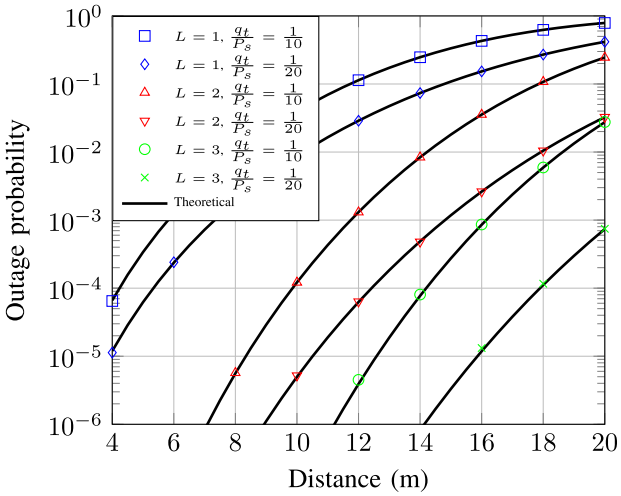

Fig. 4. Outage probability versus the distance between the PB and the EH source.

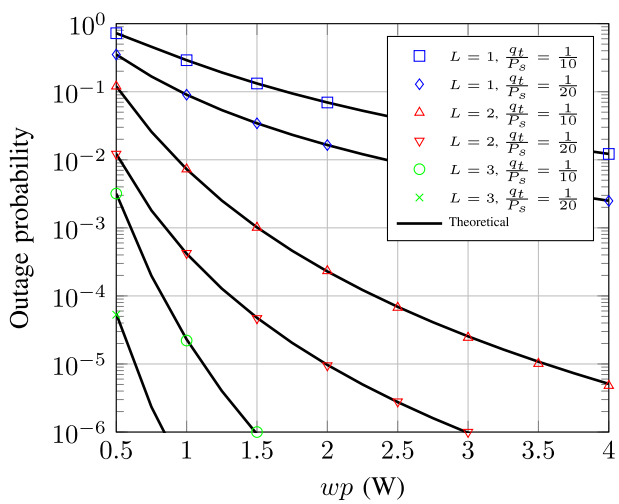

Fig. 5. Outage probability versus power *wp*.

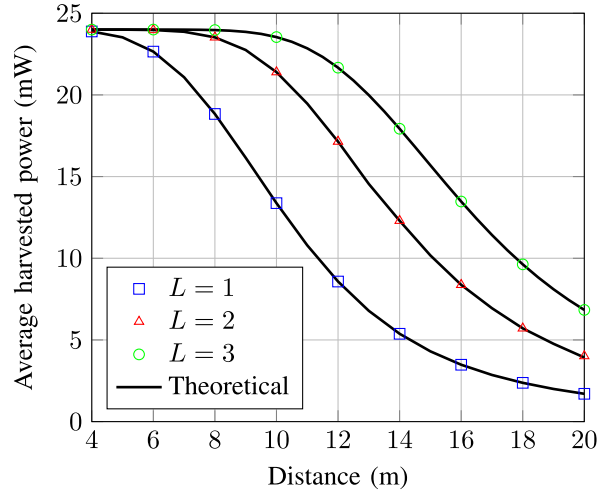

Fig. 6. Average harvested power versus the distance between the PB and the EH source.

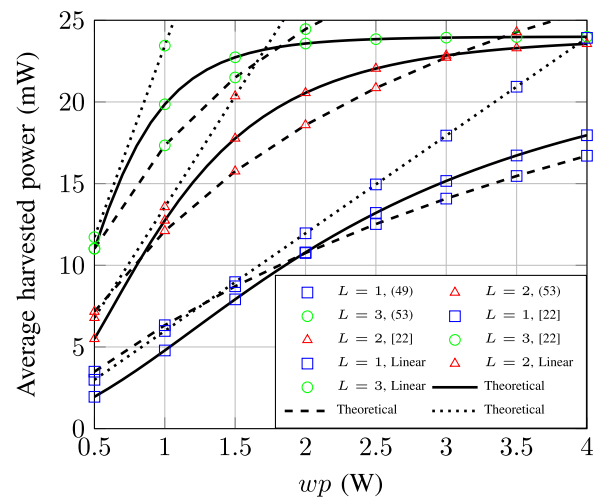

Fig. 7. Average harvested power versus power *wp*.

steeper, as L increases. The improvement of the performance, when L increases, is also illustrated in Figs. 6 and 7. For small distances in Fig. 6 and for large transmitted power in Fig. 7, the average harvested power is saturated at 24 mW, which is the value of the maximum harvested power when the power harvesting circuit is saturated. For the case of no CSI at the PBs, L times more power is needed to achieve the same performance as the one when perfect CSI is available at the PBs. Moreover, in Fig. 7 the linear model and the nonlinear model proposed in [22] are presented, highlighting the fact that the linear model cannot describe the saturation and the derived analysis is necessary to statistically investigate the nonlinear model that fits in the data provided in [39]. Therefore, the performance of the three EH models cannot be fairly compared. In all figures, it can be observed that the theoretical lines coincide with the symbols obtained from simulations.

V. Conclusion

In this work, the Pearson type III and log Pearson type III distributions have been utilized in WPT, taking into account the nonlinear relationship between the received and harvested power. Closed-form expressions for the statistical properties of a general form of the Pearson type III and the log Pearson type III distributions have been extracted and utilized to introduce the logit Pearson type III distribution, which is closely related to the considered nonlinear EH model, deriving closed-form expressions for its CDF, PDF, and moments. The distributions of the sum, the log sum, and the logit sum of Pearson type III RVs and their statistical properties have also been investigated. The derived results have been utilized to extract closed-form expressions for the CDF, the PDF, and the moments of the harvested power for an SISO and an MISO system with the considered nonlinear EH model, where either perfect CSI or no CSI is available at the PB. These statistical properties can provide useful insights such as the probability that outage occurs in the harvested power considering a specific threshold and the average harvested power by the source.

APPENDIX A
PROOF OF PROPOSITION 5

When $b_i = b \quad \forall i$, the PDF can be derived by the inverse Laplace transform of the product of the moment generation functions of the Pearson type III distribution. To derive the PDF of $\hat{X}_L$, when $b_i \neq b_j \quad \forall i \neq j$, similar steps as in [31] are followed. First, we consider the case of two terms ($L = 2$). The PDF of $\hat{X}_2 = X_1 + X_2$, considering that if $b > 0$, $x \in (m, \infty)$, can be obtained as follows:

$$f_{\hat{X}_2}(x) = \int_{m_1}^{z-m_2} f_{X_1}(y, a_1, b_1, m_1) f_{X_2}(x-y, a_2, b_2, m_2) dy. \tag{54}$$

Using $z = y - m_1$ and [32, eq. (3.383.1)], (54) can be rewritten as follows:

$$\begin{aligned} f_{\hat{X}_2}(x) = &\frac{b_1^{a_1} b_2^{a_2}}{\Gamma(a_1)\Gamma(a_2)} e^{-b_2(z-m_1-m_2)} (z-m_1-m_2)^{a_1+a_2-1} \\ &\times B(a_2, a_1) {}_1F_1(a_1; a_1+a_2; (b_2-b_1)(z-m_1-m_2)) \end{aligned} \tag{55}$$

where $B(\cdot,\cdot)$ is the Euler Beta function [32] and ${}_1F_1(\cdot;\cdot;\cdot)$ is the confluent hypergeometric function [32]. Since $a_i \in \mathbb{Z}$ and $a_i > 0$, using [40, eq. (07.20.03.0024.01)], (55) can be rewritten as follows:

$$\begin{aligned} f_{\hat{X}_2}(x) = &\frac{(1-a_1-a_2)_{a_1} (b_2-b_1)^{1-a_1-a_2} b_1^{a_1} b_2^{a_2}}{(a_1-1)!(a_1+a_2-1)!} \\ &\times \left(\sum_{k=0}^{a_2-1} \frac{(1-a_2)_k ((b_2-b_1)(z-m_1-m_2))^k}{k!(2-a_1-a_2)_k} \right. \\ &\times e^{-b_2(z-m_1-m_2)} - e^{-b_1(z-m_1-m_2)} \\ &\left. \times \sum_{k=0}^{a_1-1} \frac{(1-a_1)_k ((b_1-b_2)(z-m_1-m_2))^k}{k!(2-a_1-a_2)_k} \right) \end{aligned} \tag{56}$$

where $(n)_k$ is the Pochhammer symbol. After some algebraic manipulations, (56) can be written as follows:

$$f_{\hat{X}_2}(x) = \sum_{i=1}^{2} \sum_{k=1}^{a_i} f_{X_i}(x, k, b_i, \hat{m}_2) \Xi_2(i, k, a_1, a_2, b_1, b_2) \tag{57}$$

where

$$\begin{aligned} \Xi_2(i, k, a_1, a_2, b_1, b_2) = &(-1)^{\hat{m}_2 - m_i} \frac{b_1^{a_1} b_2^{a_2}}{b_k} \\ &\times \frac{(a_1+a_2-k-1)! \left(b_i - b_{1+U(1-i)}\right)^{k-a_1-a_2}}{\left(a_{1+U(1-i)} - 1\right)!(a_i-k)!}. \end{aligned} \tag{58}$$

It should be highlighted that if $b < 0$, $x \in (-\infty, m)$ and the PDF of $\hat{X}_2$ can be obtained as follows:

$$f_{\hat{X}_2}(x) = \int_{z-m_2}^{m_1} f_{X_1}(y, a_1, b_1, m_1) f_{X_2}(x-y, a_2, b_2, m_2) dy \tag{59}$$

which results in (57) considering that $|b|$ appears in (1).

When $L = 3$, the PDF of $\hat{X}_3 = \hat{X}_2 + X_3$ can be obtained as follows:

$$f_{\hat{X}_3}(x) = \int_{m_1+m_2}^{z-m_3} f_{\hat{X}_3}(y) f_{X_3}(x-y, a_3, b_3, m_3) dy. \tag{60}$$

Following similar steps and after some complicated algebraic manipulations, (60) can written as follows:

$$\begin{aligned} f_{\hat{X}_3}(x) = &\sum_{i=1}^{3} \sum_{k=1}^{a_i} f_{X_i}(x, k, b_i, \hat{m}_3) \\ &\times \Xi_3(i, k, a_1, a_2, a_3, b_1, b_2, b_3) \end{aligned} \tag{61}$$

where

$$\begin{aligned} \Xi_3(i, k, a_1, a_2, a_3, b_1, b_2, b_3, j_1) = &(-1)^{\hat{m}_3 - m_i} \frac{b_1^{a_1} b_2^{a_2} b_3^{a_3}}{b_k} \\ &\times \frac{(a_i+a_{1+U(1-i)}-j_1-1)!(b_i-b_{1+U(1-i)})^{j_1-a_i-a_{1+U(1-i)}}}{(a_{1+U(1-i)}-1)!(a_i-j_1)!} \\ &\times \frac{(j_1+a_{2+U(2-i)}-k-1)!(b_i-b_{2+U(2-i)})^{k-j_1-a_{2+U(2-i)}}}{(a_{2+U(2-i)}-1)!(j_1-k)!}. \end{aligned} \tag{62}$$

When $b_i < 0 \quad \forall i$, the PDF of $\hat{X}_3$ can be obtained as follows:

$$f_{\hat{X}_3}(x) = \int_{z-m_3}^{m_1+m_2} f_{\hat{X}_2}(y) f_{X_3}(x-y, a_3, b_3, m_3) dy \tag{63}$$

which results in (61).

Following similar steps for L terms, (17) is derived.

APPENDIX B
PROOF OF PROPOSITION 13

The nth moment of the logit Pearson type III distribution when $b > 0$ can be obtained by the integral $\int_{(1/1+e^{-m})}^{1} z^n f_Z(z) dz$ which can be rewritten as follows:

$$\mu_Z^n(a, b, m) = \frac{1}{\Gamma(a)} \int_0^\infty \left(\frac{1}{1+e^{-\frac{z}{b}-m}} \right)^n x^{a-1} e^{-x} dz. \tag{64}$$

When $m \geq 0$, it holds that $e^{-(z/b-m)} \leq 1$ and utilizing the binomial theorem for negative integer exponent, (64) can be rewritten as follows:

$$\begin{aligned} \mu_Z^n(a, b, m) = &\frac{1}{\Gamma(a)} \int_0^\infty \sum_{l=0}^{\infty} \binom{n+l-1}{l} (-1)^l e^{-ml} \\ &\times z^{a-1} e^{-\left(1+\frac{l}{b}\right)z} dz. \end{aligned} \tag{65}$$

The infinite series in (65) converges from the utilization of the binomial theorem. When $m \geq 0$, (30) is derived by interchanging the order of summation and integration and using the definition of the gamma function and [32, eq. (3.381.4)].

When $m < 0$, utilizing the binomial theorem for negative integer exponent, the denominator can be written as follows:

$$\left(1+e^{-\frac{z}{b}-m}\right)^{-n} = \begin{cases} \sum_{l=0}^{\infty} \binom{n+l-1}{l} (-1)^l e^{m(n+l)} e^{\frac{n+l}{b} z} & x < -mb \\ \sum_{l=0}^{\infty} \binom{n+l-1}{l} (-1)^l e^{-ml} e^{-\frac{l}{b} z} & x > -mb. \end{cases} \tag{66}$$

In this case, the nth moment can be calculated as follows:

$$\begin{aligned} \mu_Z^n(a, b, m) = &\frac{1}{\Gamma(a)} \int_0^{-mb} \sum_{l=0}^{\infty} \binom{n+l-1}{l} (-1)^l e^{m(n+l)} \\ &\times z^{a-1} e^{-\left(1-\frac{n+l}{b}\right)z} dz + \frac{1}{\Gamma(a)} \int_{-mb}^{\infty} \sum_{l=0}^{\infty} \binom{n+l-1}{l} \\ &\times (-1)^l e^{-ml} z^{a-1} e^{-\left(1+\frac{l}{b}\right)z} dz. \end{aligned} \tag{67}$$

Considering the definition of the lower and upper incomplete gamma function and [32, eqs. (3.381.1) and (3.381.3)], (30) is derived when $m < 0$ which completes the proof.

APPENDIX C
PROOF OF THEOREM 3

Setting in $\int_0^{P_s} q^n f_{Q^S}(q)dq$

$$x = -\hat{b}\left(\ln\left(\frac{c\left(1+e^{AB}\right)}{q+c} - 1\right) - AB\right) \tag{68}$$

the nth moment is calculated as follows:

$$\mu_{Q^S}^n = \frac{c^n}{\Gamma(a)}\int_0^\infty e^{-x}x^{a-1}\left(\frac{e^{-AB}+1}{e^{-x/\hat{b}}+e^{-AB}} - 1\right)^n dx. \tag{69}$$

Using the binomial theorem, (69) can be rewritten as follows:

$$\mu_{Q^S}^n = \frac{c^n}{\Gamma(a)}\sum_{l_1=0}^{n}\binom{n}{l_1}(-1)^{n-l_1}\left(e^{-AB}+1\right)^{l_1} \times \int_0^\infty \frac{x^{a-1}e^{-x}}{\left(e^{-x/\hat{b}}+e^{-AB}\right)^{l_1}}dx. \tag{70}$$

Utilizing the binomial theorem for negative integer exponent, the denominator can be written as follows:

$$\left(e^{-x/\hat{b}}+e^{-AB}\right)^{-l_1} = \begin{cases} \sum_{l_2=0}^{\infty}\binom{l_1+l_2-1}{l_2}\left(e^{-x/\hat{b}}\right)^{-l_1-l_2} \\ \quad \times (-1)^{l_2}\left(e^{-AB}\right)^{l_2}, \ x < AB\hat{b} \\ \sum_{l_2=0}^{\infty}\binom{l_1+l_2-1}{l_2}\left(e^{-AB}\right)^{-l_1-l_2} \\ \quad \times (-1)^{l_2}\left(e^{-x/\hat{b}}\right)^{l_2}, \ x > AB\hat{b}. \end{cases} \tag{71}$$

In this case, the infinite series always converge. Using (70) and (71) can be rewritten as follows:

$$\mu_{Q^S}^n = \frac{c^n}{\Gamma(a)}\sum_{l_1=0}^{n}\sum_{l_2=0}^{\infty}\binom{n}{l_1}\binom{l_1+l_2-1}{l_2}(-1)^{n-l_1+l_2} \times \left(e^{-ABl_2}\int_0^{AB\hat{b}} x^{a-1}e^{-(1-(l_1+l_2)/\hat{b})x}dx + e^{AB(l_1+l_2)}\int_{AB\hat{b}}^{\infty} x^{a-1}e^{-(1+l_2/\hat{b})x}dx\right)\left(e^{-AB}+1\right)^{l_1}. \tag{72}$$

Considering the definition of lower and upper incomplete gamma function and [32, eqs. (3.381.1) and (3.381.3)], respectively, (48) is derived.

REFERENCES

[1] S. A. Tegos, G. K. Karagiannidis, P. D. Diamantoulakis, and N. D. Chatzidiamantis, "Nonlinear energy harvesting evaluation through the logit Pearson distribution," in *Proc. IEEE 22nd Int. Workshop Signal Process. Adv. Wireless Commun. (SPAWC)*, Lucca, Italy, Nov. 2021, pp. 611–615.

[2] N. L. Johnson, S. Kotz, and N. Balakrishnan, *Continuous Univariate Distributions*. New York, NY, USA: Wiley, 1995.

[3] V. P. Singh, "Pearson type III distribution," in *Entropy-Based Parameter Estimation in Hydrology*. Dordrecht, The Netherlands: Springer, Jan. 1998.

[4] V. P. Singh, "Log-Pearson type III distribution," in *Entropy-Based Parameter Estimation in Hydrology*. Dordrecht, The Netherlands: Springer, Jan. 1998.

[5] B. Bobee, "The log Pearson type 3 distribution and its application in hydrology," *Water Resour. Res.*, vol. 11, no. 5, pp. 681–689, Oct. 1975.

[6] H. N. Phien and T. J. Ajirajah, "Applications of the log Pearson type-3 distribution in hydrology," *J. Hydrol.*, vol. 73, no. 3, pp. 359–372, Aug. 1984.

[7] I. Gupta and V. Deshpande, "Application of log-Pearson type-ill distribution for evaluating design earthquake magnitudes," *J. Inst. Eng. Civil Eng. Division*, vol. 75, pp. 129–134, Nov. 1994.

[8] Z. Shi, S. Ma, G. Yang, K.-W. Tam, and M. Xia, "Asymptotic outage analysis of HARQ-IR over time-correlated Nakagami- *m* fading channels," *IEEE Trans. Wireless Commun.*, vol. 16, no. 9, pp. 6119–6134, Sep. 2017.

[9] F. Yilmaz and M.-S. Alouini, "Product of shifted exponential variates and outage capacity of multicarrier systems," in *Proc. Eur. Wireless Conf.*, Aalborg, Denmark, May 2009, pp. 282–286.

[10] Z. Li, Y. Guo, and X. Ge, "Performance analysis of urban mmWave multi-hop V2V communications with shifted-exponential distribution headway," in *Proc. IEEE Int. Conf. Commun. Workshops (ICC Workshops)*, Shanghai, China, May 2019, pp. 1–6.

[11] S. Kim, J. Y. Lee, and D. K. Sung, "A shifted gamma distribution model for long-range dependent Internet traffic," *IEEE Commun. Lett.*, vol. 7, no. 3, pp. 124–126, Mar. 2003.

[12] K. Aghababaiyan, V. Shah-Mansouri, and B. Maham, "Capacity and error probability analysis of neuro-spike communication exploiting temporal modulation," *IEEE Trans. Commun.*, vol. 68, no. 4, pp. 2078–2089, Apr. 2020.

[13] A. Brékine *et al.*, "Building a roadmap for the next generation Internet of Things. Research, innovation and implementation 2021–2027," Scoping Paper, Sep. 2019.

[14] P. D. Diamantoulakis, "Resource allocation in wireless networks with energy constraints," Ph.D. dissertation, Dept. Electr. Comput. Eng. Telecommun., Aristotle Univ. Thessaloniki, Thessaloniki, Greece, 2017.

[15] P. Grover and A. Sahai, "Shannon meets tesla: Wireless information and power transfer," in *Proc. IEEE Int. Symp. Inf. Theory*, Austin, TX, USA, Jun. 2010, pp. 2363–2367.

[16] I. Krikidis, "Wireless power transfer under Kullback-Leibler distribution uncertainty: A mathematical framework," *IEEE Wireless Commun. Lett.*, vol. 9, no. 9, pp. 1591–1595, Sep. 2020.

[17] X. Zhou, R. Zhang, and C. K. Ho, "Wireless information and power transfer in multiuser OFDM systems," *IEEE Trans. Wireless Commun.*, vol. 13, no. 4, pp. 2282–2294, Apr. 2014.

[18] S. A. Tegos, P. D. Diamantoulakis, A. S. Lioumpas, P. G. Sarigiannidis, and G. K. Karagiannidis, "Slotted ALOHA with NOMA for the next generation IoT," *IEEE Trans. Commun.*, vol. 68, no. 10, pp. 6289–6301, Oct. 2020.

[19] L. Xiao, Y. Li, C. Dai, H. Dai, and H. V. Poor, "Reinforcement learning-based NOMA power allocation in the presence of smart jamming," *IEEE Trans. Veh. Technol.*, vol. 67, no. 4, pp. 3377–3389, Apr. 2018.

[20] P. D. Diamantoulakis, K. N. Pappi, Z. Ding, and G. K. Karagiannidis, "Wireless-powered communications with non-orthogonal multiple access," *IEEE Trans. Wireless Commun.*, vol. 15, no. 12, pp. 8422–8436, Dec. 2016.

[21] E. Boshkovska, D. W. K. Ng, N. Zlatanov, and R. Schober, "Practical non-linear energy harvesting model and resource allocation for SWIPT systems," *IEEE Commun. Lett.*, vol. 19, no. 12, pp. 2082–2085, Dec. 2015.

[22] Y. Chen, N. Zhao, and M.-S. Alouini, "Wireless energy harvesting using signals from multiple fading channels," *IEEE Trans. Commun.*, vol. 65, no. 11, pp. 5027–5039, Nov. 2017.

[23] B. Clerckx, "Wireless information and power transfer: Nonlinearity, waveform design, and rate-energy tradeoff," *IEEE Trans. Signal Process.*, vol. 66, no. 4, pp. 847–862, Feb. 2018.

[24] J.-M. Kang, I.-M. Kim, and D. I. Kim, "Wireless information and power transfer: Rate-energy tradeoff for nonlinear energy harvesting," *IEEE Trans. Wireless Commun.*, vol. 17, no. 3, pp. 1966–1981, Mar. 2018.

[25] B. Clerckx, R. Zhang, R. Schober, D. W. K. Ng, D. I. Kim, and H. V. Poor, "Fundamentals of wireless information and power transfer: From RF energy harvester models to signal and system designs," *IEEE J. Sel. Areas Commun.*, vol. 37, no. 1, pp. 4–33, Jan. 2019.

[26] S. A. Tegos, P. D. Diamantoulakis, K. N. Pappi, P. C. Sofotasios, S. Muhaidat, and G. K. Karagiannidis, "Toward efficient integration of information and energy reception," *IEEE Trans. Commun.*, vol. 67, no. 9, pp. 6572–6585, Sep. 2019.

[27] N. L. Johnson, "Systems of frequency curves generated by methods of translation," *Biometrika*, vol. 36, nos. 1–2, pp. 149–176, Jun. 1949. [Online]. Available: https://doi.org/10.1093/biomet/36.1-2.149

[28] P. Frederic and F. Lad, "Two moments of the logitnormal distribution," *Commun. Stat. Simul. Comput.*, vol. 37, no. 7, pp. 1263–1269, Feb. 2008.
[29] G. K. Karagiannidis, "Moments-based approach to the performance analysis of equal gain diversity in Nakagami-m fading," *IEEE Trans. Commun.*, vol. 52, no. 5, pp. 685–690, May 2004.
[30] C. A. Coelho, "The generalized integer gamma distribution—A basis for distributions in multivariate statistics," *J. Multivariate Anal.*, vol. 64, no. 1, pp. 86–102, Jan. 1998.
[31] G. K. Karagiannidis, N. C. Sagias, and T. A. Tsiftsis, "Closed-form statistics for the sum of squared Nakagami-m variates and its applications," *IEEE Trans. Commun.*, vol. 54, no. 8, pp. 1353–1359, Aug. 2006.
[32] I. S. Gradshteyn and I. M. Ryzhik, *Table of Integrals, Series, and Products*. San Diego, CA, USA: Academic, 2014.
[33] M. Vu, "MISO capacity with per-antenna power constraint," *IEEE Trans. Commun.*, vol. 59, no. 5, pp. 1268–1274, May 2011.
[34] C. Zhong, X. Chen, Z. Zhang, and G. K. Karagiannidis, "Wireless-powered communications: Performance analysis and optimization," *IEEE Trans. Commun.*, vol. 63, no. 12, pp. 5178–5190, Dec. 2015.
[35] H. Ju and R. Zhang, "A novel mode switching scheme utilizing random beamforming for opportunistic energy harvesting," *IEEE Trans. Wireless Commun.*, vol. 13, no. 4, pp. 2150–2162, Apr. 2014.
[36] E. A. Jorswieck and H. Boche, "Optimal transmission strategies and impact of correlation in multiantenna systems with different types of channel state information," *IEEE Trans. Signal Process.*, vol. 52, no. 12, pp. 3440–3453, Dec. 2004.
[37] Z. Hadzi-Velkov, S. Pejoski, N. Zlatanov, and R. Schober, "Proportional fairness in ALOHA networks with RF energy harvesting," *IEEE Wireless Commun. Lett.*, vol. 8, no. 1, pp. 277–280, Feb. 2019.
[38] E. Boshkovska, N. Zlatanov, L. Dai, D. W. K. Ng, and R. Schober, "Secure SWIPT networks based on a non-linear energy harvesting model," in *Proc. IEEE Wireless Commun. Netw. Conf. Workshops (WCNCW)*, San Francisco, CA, USA, Mar. 2017, pp. 1–6.
[39] J. Guo and X. Zhu, "An improved analytical model for RF-DC conversion efficiency in microwave rectifiers," in *IEEE/MTT-S Int. Microw. Symp. Dig.*, Montreal, QC, Canada, Jun. 2012, pp. 1–3.
[40] "The Mathematical Functions Site." 2022. [Online]. Available: https://functions.wolfram.com/

Sotiris A. Tegos (Student Member, IEEE) received the Diploma (five years) and the Ph.D. degrees in electrical and computer engineering from the Aristotle University of Thessaloniki (AUTH), Thessaloniki, Greece, in 2017 and 2022, respectively.

Also, he is a member of the Wireless Communications and Information Processing Group, AUTH. In 2018, he was a Visitor Researcher with the Department of Electrical and Computer Engineering, Khalifa University, Abu Dhabi, UAE. His current research interests include wireless power transfer, probability theory, and multiple access in wireless communications.

Dr. Tegos was an Exemplary Reviewer in IEEE WIRELESS COMMUNICATIONS LETTERS in 2019 (top 3% of reviewers).

George K. Karagiannidis (Fellow, IEEE) received the University Diploma (five years) and Ph.D. degrees in electrical and computer engineering from the University of Patras, Patras, Greece, in 1987 and 1999, respectively.

He is currently a Professor with the Electrical and Computer Engineering Department and the Head of Wireless Communications and Information Processing Group, Aristotle University of Thessaloniki, Thessaloniki, Greece. He is also the Honorary Professor with South West Jiaotong University, Chengdu, China. His research interests are in the broad area of digital communications systems and signal processing.

Prof. Karagiannidis received the 2021 IEEE Communications Society Radio Communications Committee Technical Recognition Award and the 2018 Signal Processing and Communications Electronics Technical Recognition Award of the IEEE Communications Society. He is one of the highly-cited authors across all areas of Electrical Engineering, recognized from Clarivate Analytics as Web-of-Science Highly-Cited Researcher in the last seven consecutive years 2015–2021. In the past, he was the Editor-in-Chief of IEEE COMMUNICATIONS LETTERS from 2012 to 2015 and the Associate Editor-in-Chief of IEEE OPEN JOURNAL OF THE COMMUNICATIONS SOCIETY from 2019 to 2022.

Panagiotis D. Diamantoulakis (Senior Member, IEEE) received the Diploma (five years) and Ph.D. degrees from the Department of Electrical and Computer Engineering, Aristotle University of Thessaloniki (AUTH), Thessaloniki, Greece, in 2012 and 2017, respectively.

Since 2017, he has been working as a Postdoctoral Fellow with the Wireless Communications and Information Processing Group, AUTH and since 2021, he has been a Visiting Assistant Professor with the Key Lab of Information Coding and Transmission, Southwest Jiaotong University, Chengdu, China. His research interests include optimization theory and applications in integrated communication and computing networks, optical wireless communications (OWC) and hybrid OWC/RF networks, and wireless power transfer.

Dr. Diamantoulakis serves as an Editor for IEEE WIRELESS COMMUNICATIONS LETTERS, IEEE OPEN JOURNAL OF THE COMMUNICATIONS SOCIETY, *Physical Communication* (Elsevier), and *Frontiers in Communications and Networks*. He was also an Exemplary Editor of IEEE WIRELESS COMMUNICATIONS LETTERS in 2020, an Exemplary Reviewer of IEEE COMMUNICATIONS LETTERS in 2014 and IEEE TRANSACTIONS ON COMMUNICATIONS in 2017 and 2019. He is a Working Group Member of the Newfocus COST Action "European Network on Future Generation Optical Wireless Communication Technologies."

Nestor D. Chatzidiamantis (Senior, Member IEEE) was born in Los Angeles, CA, USA, in 1981. He received the Diploma degree (five years) in electrical and computer engineering (ECE) from the Aristotle University of Thessaloniki (AUTH), Thessaloniki, Greece, in 2005, the M.Sc. degree in telecommunication networks and software from the University of Surrey, Guildford, U.K., in 2006, and the Ph.D. degree from the ECE Department, AUTH in 2012.

From 2012 to 2015, he worked as a Postdoctoral Research Associate with AUTH and from 2016 to 2018, as a Senior Engineer with Hellenic Electricity Distribution Network Operator, Attica, Greece. Since 2018, he has been an Assistant Professor with the ECE Department, AUTH and a member of the Telecommunications Laboratory. His research areas span signal processing techniques for communication systems, performance analysis of wireless communication systems over fading channels, communications theory, cognitive radio, and free-space optical communications.